J. Fluid Mech. (1987), *vol.* 185, *pp.* 137–151
Printed in Great Britain

Experimental studies of wakes behind circularly capped bubbles

By W. F. BESSLER AND H. LITTMAN
Department of Chemical Engineering, Rensselaer Polytechnic Institute,
Troy, NY 12180-3590, USA

(Received 17 October 1985 and in revised form 15 April 1987)

The wake behind a circularly capped bubble rising in fluids of different viscosity has been experimentally investigated using aspirin powder for flow visualization and high-speed photography synchronized with pressure–time measurements to measure the pressure field. The bubble plus its primary wake with a cusped tail is observed to contain symmetric pressure minima within the primary wake. Adjacent to the boundary wake is a free shear layer which contains large-scale vortices generated near the bubble rim that remain essentially stationary to an observer in the laboratory reference frame. The change in wake geometry and the transition to an ellipsoidal bubble shape as fluid viscosity increases is documented.

The airfoil shape of the boundary of the circularly capped bubble and its closed primary wake is modelled using a Joukowski transformation in which the Joukowski constant is adjusted to match the experimental and potential-flow pressures along the bubble cap. The model successfully predicts the frontal pressure field, and the wake size and shape. The Davies & Taylor bubble-cap boundary condition is also verified.

1. Introduction

The key role that bubbles play in many chemical and physical processes has led to the analysis of the flow field around them. Flow visualization studies of the wake have been conducted to determine its shape, whether it is open or closed and the conditions under which it is laminar and turbulent. Previous investigations are not in complete agreement with regard to all of these matters.

Spherical cap (three-dimensional) and circular cap (two-dimensional) bubbles occur at high Reynolds and Weber (or Eotvos)† numbers. Unless otherwise stated in this paper, the dimensionless groups mentioned are based on the bubble's rise velocity U, and the equivalent sphere (three-dimensional) or cylinder (two-dimensional) radius r_e. To be explicit, $Re = 2r_e U/\nu$, where ν is the kinematic viscosity of the liquid and $We = 2r_e \rho U^2/\sigma$ where ρ is the density of the liquid and σ is its surface tension.

Haberman & Morton (1953) found that the transition to a spherical cap geometry was complete at a Weber number of 20. From their figure 21, C_D becomes constant for Weber numbers above about 40. For large Weber numbers, Wegener & Parlange (1973) show that the Froude number ($Fr = U/(gr_e)^{\frac{1}{2}}$, where g is the gravitational acceleration) varies from 1 to 1.05 for Re greater than about 100, and below that value Fr increases with Re. (It is fairly arbitrary whether the demarking Re is 50 or

† The shape regime diagram given by Clift, Grace & Weber (1978) plots Reynolds number *vs.* Eotvos number.

100.) They also show that when Fr is not constant, geometric similarity no longer prevails and the maximum angle θ_m increases as Re is lowered. Above $Re = 100$, θ_m is about 50° where θ_m is the angle between the polar axis and the radius to the bubble rim.

Wegener & Parlange (1973) have published schlieren photographs of spherical-cap bubbles rising in mineral oil at $Re = 40$, 90 and 180 which show a stable laminar primary wake with a toroidal vortex at the lowest Reynolds number. The transition to turbulence in the wake has begun by $Re = 90$ and the wake is certainly turbulent by $Re = 5100$. Slaughter & Wraith (1968) show an air bubble rising in water at $Re = 56.3$ with a closed wake inside which is a toroidal vortex. Coppus, Rietema & Ottengraf (1977) found in their work that the transition occurs at Re between 250 and 500. Since the energy dissipation process in the wake must be turbulent when the rise velocity is independent of the liquid properties (Batchelor 1967), comparison of Wegener & Parlange's Fr *vs.* Re data with the schlieren wake photographs indicates that Fr is approximately constant in the transition region. Calculation of the Fr *vs.* Re relationship for Crabtree & Bridgwater's (1967) circular-capped bubbles indicates that Fr becomes independent of Re when Re exceeds about 300.

Collins (1974) proposed a model for the flow at high Re which consists of an outer irrotational flow and a wake composed of two parts: (i) an approximately spherical surface including the bubble, its thin boundary layer, and a closed primary wake and (ii) a secondary wake emanating from the rear of the primary region with a spreading tail along its rise path. The primary wake contains a stable vortex pair that moves with the bubble. The schlieren photographs of Wegener & Parlange (1973) and the experiments of Coppus *et al.* (1977) indicate that this general picture of the bubble and its primary wake applies when the primary wake is laminar.

There is experimental evidence to support the Collins model for both spherical- and circular-capped bubbles at high Re. Lazarek & Littman's (1974) pressure-field data (two-dimensional) beneath the bubble support Collins' visual wake studies in that their pressure minima below the bubble occur inside a vertically elongated oval primary-wake boundary close to the vortex centres shown in Collins (1966). However, as discussed later, the wake can be an open helical vortex street if the bubble rocks back and forth as a result of the type of injector used. Hills (1975) also observed a vertically elongated closed primary wake during the initial stage of the bubble's rise. Spherical-cap bubbles with a closed primary wake have been observed by Davies & Taylor (1950), Slaughter & Wraith (1968), Collins (1974) and Coppus *et al.* (1977).

The works of Davies & Taylor (1950), Wegener, Sundell & Parlange (1971), Coppus *et al.* (1977) and the aforementioned argument of Batchelor (1967) show that the primary wake is turbulent at high Reynolds numbers. Turbulent primary wakes show recirculation (Collins 1965 (two-dimensional) and Coppus *et al.* 1977 (three-dimensional)). Indirect evidence of a recirculating wake in a two-dimensional bubble is inherent in the work of Lazarek & Littman (1974). Although schlieren photographs do not indicate the structure of the flow in the wake on a scale larger than that of turbulence, observation of small satellite bubbles moving with the main bubble by Wegener & Parlange (1973, p. 88) also indicate that there is recirculation in a turbulent primary wake. All this disagrees with the work of Maxworthy (1967) who found an open turbulent wake. Collins (1974), however, argues that Maxworthy's bubbles are too small to be considered spherical cap.

The primary-wake structure which emerges is not much different from that

proposed by Batchelor (1956*a*,*b*) for laminar wakes behind bluff bodies at large Reynolds number. He argues that the Helmholtz–Kirchhoff free-streamline model is wrong in concept if the wake is open, and if it is closed that viscous stresses at the boundary of the bubble would build up an appreciable circulation in the primary wake so the model would not be self-consistent. The Helmholtz free-streamline theory applied to a large gas bubble by Rippin & Davidson (1967) gives a rise velocity which is about 20% too large even though the constant-pressure condition along the cap is satisfied. This is because the pressure below the bubble floor is assumed to be that for a stagnant fluid. In an actual bubble, there is a nonlinear pressure recovery below the bubble (Lazarek & Littman 1974) and this would account for the actual rise being lower than that calculated from the model of Rippin & Davidson (1967). Collins (1974) maintains that the open infinite wake model for bubbles with high *We* and *Re* such as that calculated by Rippin & Davidson (1967), using an improved version of the model used by Moore (1959), does not even give useful approximations to the frontal flow field because it does not agree with the instantaneous streamline pattern that is observed experimentally. An excellent discussion of wakes behind spherical-cap bubbles is given by Harper (1972).

Lazarek & Littman (1974), who measured the pressure field around a large circularly capped air bubble whose wake was undoubtedly turbulent, provide strong support for the Collins model. They found the actual frontal flow well approximated by irrotational flow around an oval body. The front part of their oval corresponds to the bubble cap while the remaining portion of the oval provides a first approximation of the streamlines that leave the bubble rim and form the boundaries of the wake. Good agreement was obtained between the calculated and experimental fields when the wake boundary was allowed to take the oval form. Relatively poor agreement with the data occurred when the boundary degenerated to that of a cylinder or had an extremely large axial length like that of an open infinite wake. Further, the Davies & Taylor boundary condition along the cap was verified and as has been mentioned the pressure minima observed inside the region approximated by Collins' wake boundary were close to his vortex centres.

Ryskin & Leal (1984) developed a numerical technique to solve axisymmetric free-boundary problems and used it to predict bubble shapes and streamlines at low *Re* and *We*. However, relatively little has been done analytically or numerically at high *Re* and *We* to elucidate the details of the wake. It is worth mentioning that Saffman & Tanveer (1984) have noted that the existence of symmetrical Prandlt–Batchelor flows with two counter-rotating eddies is still an open question.

In this paper, we report experiments conducted using aspirin powder as a tracer and pressure–time measurements around the rising bubble to characterize the wake behind a circularly capped bubble. Specifically, we have investigated the shape of the primary wake, whether it is open or closed, and the nature of the flow field in the primary-wake region as a function of bubble Reynolds number. Mixtures of water and glycerine in varying proportions were used to study the effects of viscosity.

Experimental pressure data and flow visualization photographs are used to verify our wake model. The cusp-shaped primary wake first proposed by Batchelor (1956*a*, *b*) is mapped into a cylinder using the Joukowski transformation as a means of deriving its pressure field.

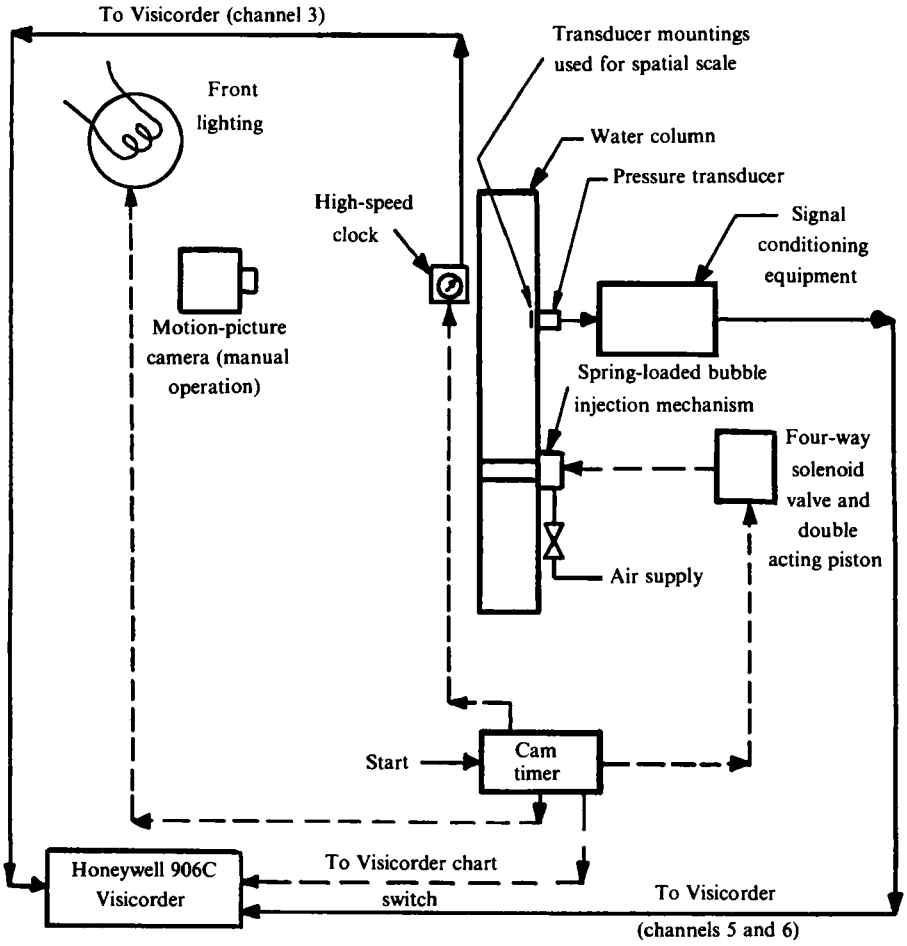

FIGURE 1. Schematic diagram of the experimental apparatus.

2. Experimental apparatus

A schematic diagram of the experimental apparatus is shown in figure 1. It is essentially the same as that used by Lazarek & Littman (1974). The parallel-plate column was constructed using a 25.4 mm thick Plexiglas front plate and a black anodized aluminium back plate set 12.7 mm apart. The space occupied by the fluid was 1.75 m high, 0.91 m wide and 12.7 mm thick. A Walters & Davidson (1962) plunger-type injector was used to inject single 'two-dimensional' bubbles (equivalent diameter: 50.8 mm) into the column. A 50 cc syringe was used to inject the aspirin powder tracer into the fluid at a point 0.71 m above the bubble injector. This allowed sufficient distance for the bubble to achieve a constant rise velocity.

The wake structure resulting from the passage of the bubble through the aspirin powder was photographed with a 16 mm Hycam high-speed camera operated at 200 frames/s and a Canon A-1 35 mm camera with a motor drive operated at 5 frames/s. DISA 51F32 pressure transducers flush mounted in the rear wall of the column at several horizontal locations were used to measure the pressure field. Synchronization

Composition % Glycerine	Temperature T (°C)	Index of refraction n_D^{20}	Density ρ (kg/m^3)	Kinematic viscosity ν (m^2/s $\times 10^6$)
99.2	24.1	1.4731	1258	908
97.9	25.4	1.4692	1253	609
95.8	23.5	1.4670	1248	553
92.4	25.3	1.4615	1240	315
87.7	25.3	1.4550	1227	116
84.9	26.3	1.4517	1220	74.3
79.0	25.2	1.4389	1205	41.2
73.3	25.0	1.4348	1189	23.9
65.1	25.2	1.4216	1167	12.4
55.2	25.3	1.4027	1139	6.66
0	26.1	1.3333	998.2	1.00

TABLE 1. Measured properties of glycerine–water mixtures

Composition % Glycerine	Bubble rise velocity U (m/s)	Aspect ratio h/a	Drag coefficient C_D	Bubble shape	Reynolds number Re	Weber number We	Froude number Fr
99.2	0.203	1.50	18.9	e	11.4	44	0.408
97.9	0.269	1.40	10.8	e	22.4	77	0.539
95.8	0.287	1.20	9.55	e–cc, f	26.4	87	0.574
92.4	0.363	0.85	5.94	cc, f	58.5	139	0.727
87.7	0.429	0.68	4.23	cc, f	188	194	0.862
84.9	0.442	0.67	3.99	cc, f	302	202	0.887
79.0	0.467	0.58	3.57	cc, f	576	223	0.938
73.3	0.500	0.56	3.11	cc, f	1063	253	1.01
65.1	0.511	0.52	2.99	cc, w	2093	255	1.03
55.2	0.521	0.50	2.90	cc, w	3974	256	1.04
0	0.526	0.47	2.82	cc, w	26721	258	1.06

TABLE 2. Measured bubble parameters in glycerine–water mixtures: e, ellipsoidal; cc, circularly capped; f, flat bubble floor; w, wavy bubble floor

of the photographs and pressure–time measurements was achieved by including a high-speed clock in the camera's field of view. Details of the equipment and experimental procedures are given in Bessler (1984).

3. Experimental data

3.1. *Fluid properties, bubble shape and drag coefficient*

Table 1 lists the measured properties of the glycerine–water mixtures used in this study. The composition of the fluid was obtained from the measured index of refraction, n_D^{20}. The density was determined using a Weld-type pycnometer and the kinematic viscosity was measured with a capillary viscometer. Average experimental values of the bubble rise velocity, aspect ratio (bubble height/bubble half-width, h/a), and the drag coefficient are presented in table 2 along with a specification of

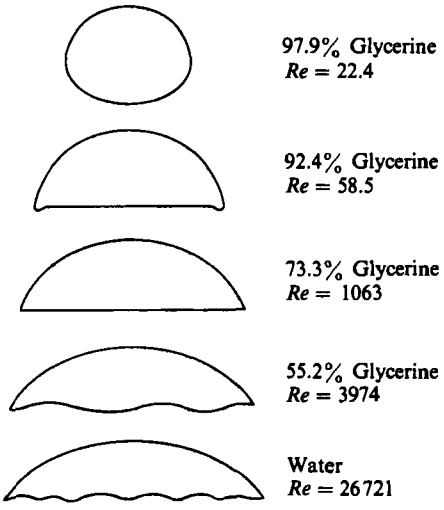

FIGURE 2. Bubble shape as a function of fluid composition – constant bubble volume.

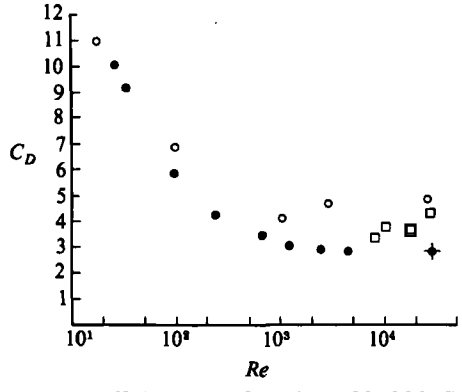

FIGURE 3. Experimental drag coefficient as a function of bubble Reynolds number: ○, Crabtree & Bridgwater (1967); □, Maneri & Mendelson (1968); +, Lazarek (1972); ●, data from table 2.

the observed bubble shape and the dimensionless parameters Re, We and Fr. Representative bubble shapes drawn from 35 mm photographs are shown in figure 2. The circularly capped bubble exhibits a wavy bubble floor at high Reynolds numbers which gradually becomes flat as fluid viscosity increases. With a further increase in viscosity, the transition to an ellipsoidal shape occurs as inertial forces become less important.

Figure 3 shows the drag coefficients, based on the equivalent bubble diameter, as a function of Re for the circularly capped bubbles observed in this study and for those reported in the literature (Crabtree & Bridgwater 1967; Maneri & Mendelson 1968; Lazarek 1972). The monotonic decrease of the drag coefficient to a constant value as Re increases is similar to the trends previously observed for spherically capped bubbles in high M ($M = g\mu^4/\rho\sigma^3$) liquids (Haberman & Morton 1953). Crabtree & Bridgwater's data are high relative to ours probably because their dump cup bubble injector causes alternate vortex shedding in the wake and a rocking motion of the bubble. In contrast, our retractable bubble injection cylinder produced a closed primary wake with no rocking of the bubble.

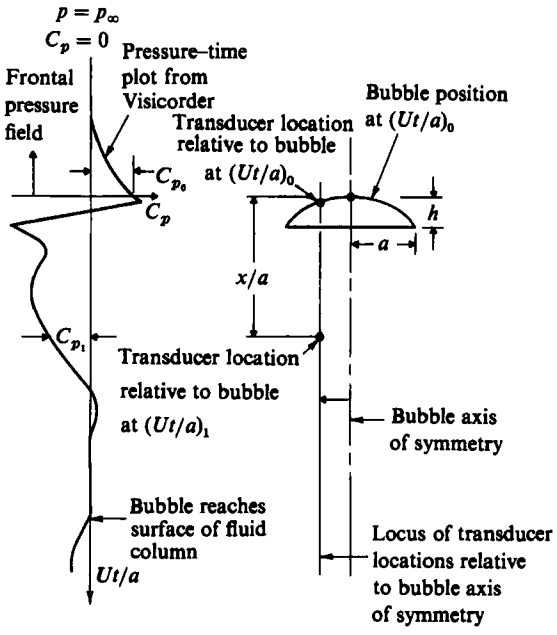

FIGURE 4. Bubble position relative to experimental pressure–time plots.

3.2. *Pressure–time traces*

The pressure–time traces for each experimental run were synchronized with the flow visualization photographs and reduced to dimensionless form using a pressure coefficient

$$C_p \equiv \frac{p - p_\infty}{\frac{1}{2}\rho U^2}, \tag{3.1}$$

where p_∞ is the static elevation head of the fluid above the transducer. Figure 4 shows a plot of C_p *vs.* the normalized time Ut/a for a bubble displaced a distance y/a from the bubble's axis of symmetry. Since the bubble is rising at its terminal velocity and the pressure inside is uniform, C_p falls linearly with time as the bubble passes the transducer.

Figure 5(*a*) shows typical pressure–time plots at $y/a = 0$ for a bubble rising in water and three different glycerine–water mixtures. The pressure–time plots in figure 5(*b*) for water show the effect of locations relative to the bubble's axial centreline. In the case of water, C_p at the stagnation point approaches the theoretical value of unity that one would expect for a two-dimensional flow around the bubble. The pressure plot for water also shows a sharp minimum and localized recovery immediately beneath the bubble floor. This behaviour can be correlated with the appearance of a wavy bubble floor and a nearly constant drag coefficient, indicating that the flow within the closed primary wake is a recirculating turbulent flow.

In the vicinity of the bubble floor, the pressure field is characterized by small lateral and large axial gradients. Note that the pressure remains the same as that inside the bubble for about six tenths of a bubble height. This is illustrated in figure 5(*a*) by the linear portion of the pressure–time curve between the bubble floor $Ut/a = 0.47$ and $Ut/a \sim 0.75$ where the pressure coefficient reaches its minimum value. In the lateral direction the linear effect extends about 1.2 bubble half-widths on either side of the bubble's axis of symmetry.

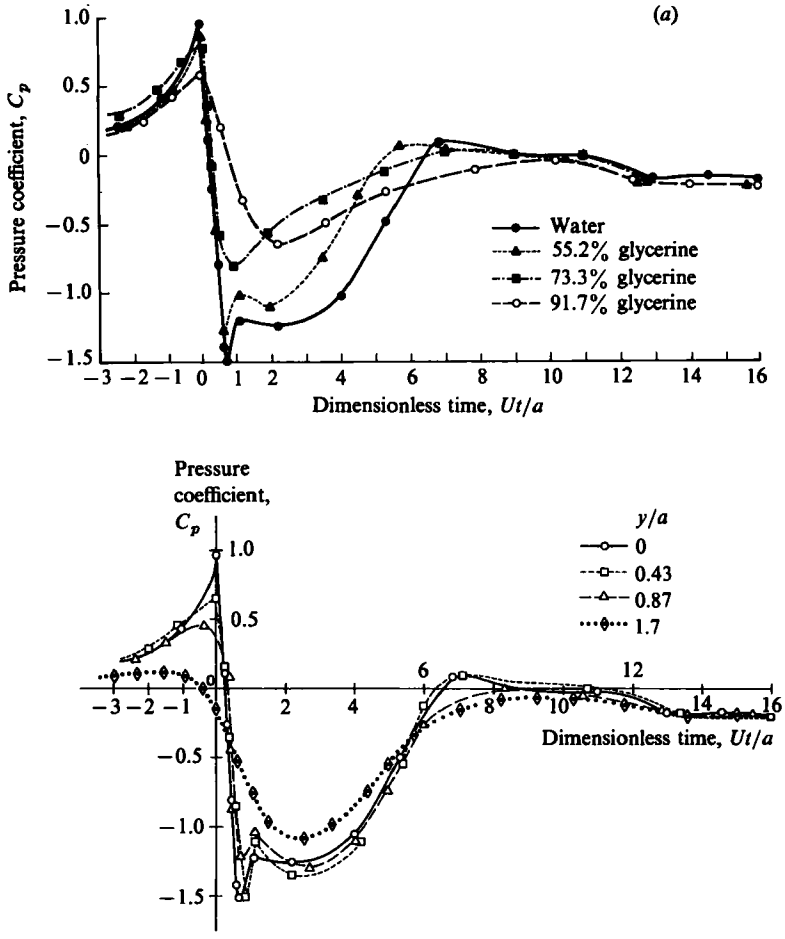

FIGURE 5 Axial pressure distribution: (*a*) along $y/a = 0$ for bubbles rising in water and glycerine; (*b*) along $y/a = 0$, 0.43, 0.87, 1.7 for bubbles rising in water.

3.3. *Effect of fluid viscosity*

Bubbles rising in 55.2% glycerine and in pure water behave similarly. They are circularly capped with a rippled floor and as seen in figure 5(*a*) the axial pressure distributions in the wake at $y/a = 0$ follow the same pattern. The length of the primary wake is about six bubble half-widths although in terms of actual length the bubble rising in pure water is slightly longer. The increase in viscosity narrows the primary wake but the shear layer adjacent to it grows at a faster rate.

In 73.3% glycerine, the bubble floor is no longer rippled (figure 2). The pressure gradient just below the bubble floor, the magnitude of the pressure minimum in the primary wake behind the bubble and the size of the primary wake are all smaller than in the lower viscosity fluids. Some three-dimensional flow is evident since C_p at the bubble nose is only 0.75. However, Fr is essentially 1 (table 2) indicating that the dissipation in the wake is still turbulent.

The corners of the bubble cap become rounded in 92.4% glycerine as shown in figure 2 and the flow around the cap begins to turn under the bubble. At the same time the shear layer develops at the corners as in less viscous fluids (although not as

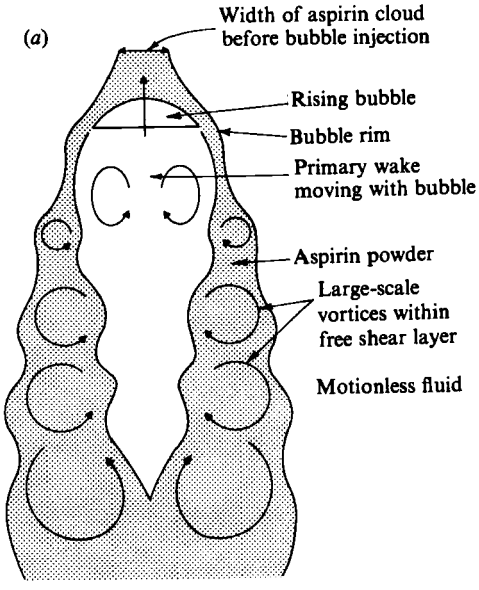

(b)

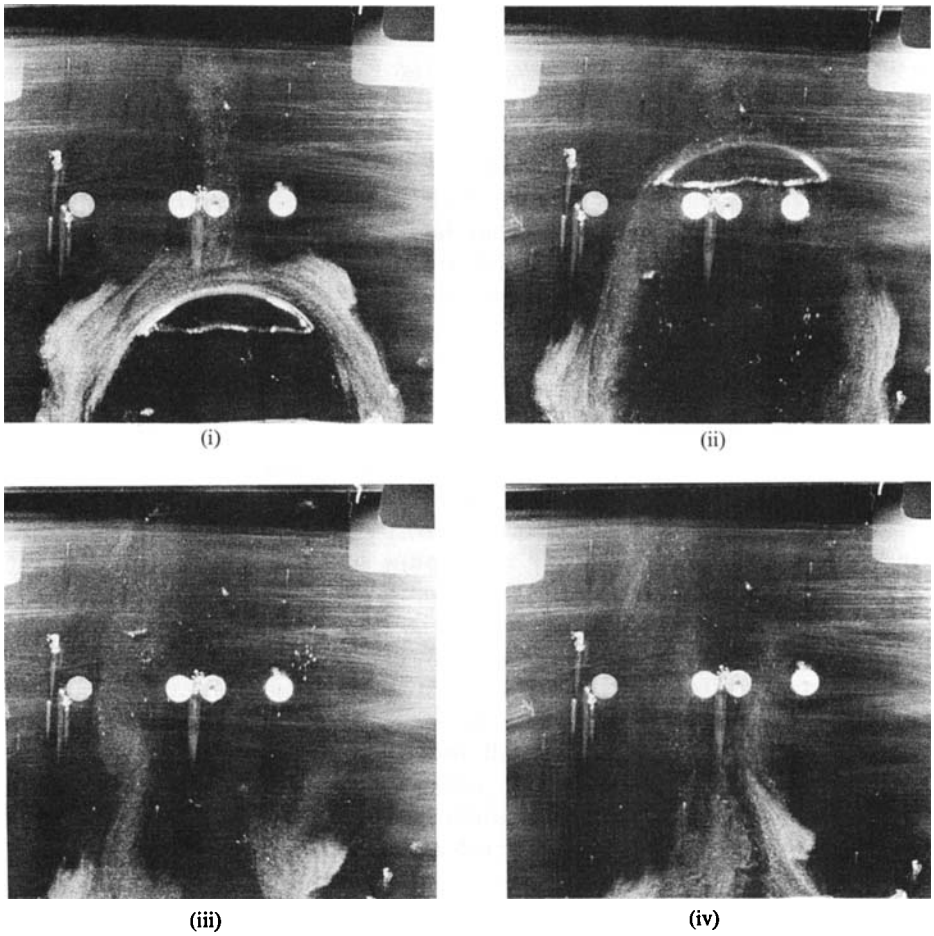

FIGURE 6. (*a*) Typical wake structure for a circularly capped bubble. (*b*) Photographs of bubble rising in water showing the outline of the primary wake. Time between photographs is 0.2 s. Aspirin powder tracer. Figure 6(*b*)(iv) shows cusp-shaped closure of primary wake.

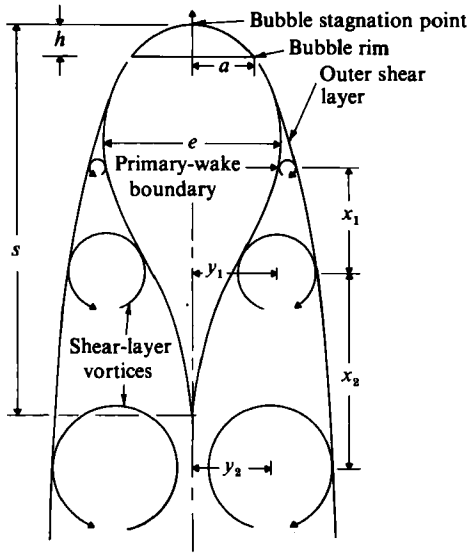

FIGURE 7. Flow geometry parameters of the primary wake and free shear layer.

intensely). The change to a more laminar wake has occurred as Fr reaches about 0.7. The axial pressure distribution is much like the curve in 73.3% glycerine. The pressure gradient just below the bubble floor is smaller in the higher viscosity fluids because of the laminar wake and lower Fr.

The bubble adopts an ellipsoidal shape in 97.9% glycerine as the surface-tension force becomes more significant. The shear layer associated with circularly capped bubbles is no longer observed and the flow around the bubble appears laminar with the aspirin following streamlines about the ellipsoidal shape. Three-dimensional flow near the bubble nose is substantial.

3.4. *Wake phenomena*

Closed primary wakes behind bubbles are typically idealized as being separated from the outer flow field by a single dividing streamline (Lazarek & Littman 1974). However, if one assumes an oval wake shape consistent in size with experimental pressure traces, a rough calculation of the energy dissipation within the primary wake indicates that it is insufficient to account for the observed rise velocities. Additional energy must somehow be dissipated elsewhere in the flow field.

The general features of the flow behind the bubble obtained from high-speed photographs of the bubble using aspirin powder for visualization of the flow are shown diagrammatically in figure 6(*a*). Figure 6(*b*) shows a sequence of 35 mm photographs of the bubble rising in pure water. The aspirin visible below the bubble floor was trapped between the front wall and the bubble as it passed through the aspirin cloud. Adjacent to the primary wake is a free shear layer which contains large-scale vortices generated near the bubble rim that remain essentially stationary relative to an observer in the laboratory reference frame. There is no flow of aspirin into the primary wake through the shear layer. The liquid clear of aspirin in figure 6(*a*) is assumed to be the primary wake and the liquid containing aspirin is identified with the shear layer. In a frame moving with the bubble, the shed vortex centres would be seen as moving away from the bubble at velocity U. The vortices are

Quantity	Water	% Glycerine 58.5	73.7	91.7
Rise velocity U(m/s)	0.53	0.52	0.50	0.38
Bubble width $2a$(m)	0.12	0.11	0.11	0.091
Bubble height h(m)	0.027	0.029	0.31	0.037
Aspect ratio h/a	0.47	0.51	0.57	0.81
Wake length $s-h$(m)	0.36	0.35	0.30	0.27
Wake width e(m)	0.18	0.16	0.13	0.088
Vortex Spacing				
x_1(m)	0.083	0.092	0.093	0.082
y_1(m)	0.099	0.091	0.089	0.055
x_2(m)	0.084	0.095	0.099	0.079
y_2(m)	0.098	0.089	0.085	0.048

TABLE 3. Measured wake parameters in glycerine–water mixtures

periodically generated as the bubble and its primary-wake fluid rise upward through the motionless fluid in the column. As the vortices dissipate energy, they grow in size causing the primary wake to adopt an airfoil shape with a cusped tail. The absence of aspirin in the wake region directly behind the bubble shows, in agreement with Collins (1966), that a closed primary wake does indeed exist. Within the primary wake, the general trend of the pressure traces coupled with photographs of occasional stray particles trapped in this region indicate that a recirculation pattern is generated by a vortex pair symmetrically placed about the wake centreline. The velocity of the fluid inside the wake relative to the bubble is much smaller than the rise velocity.

Based on these experimental observations, the wake geometry was characterized using the parameters shown in figure 7. Measured values presented in table 3 demonstrate the influence of viscosity on the geometry of the wake. Specifically, as the fluid viscosity increases, the shear layers develop more rapidly and the size of the primary wake decreases. The spacing of the vortex centres is relatively insensitive to viscosity and they remain more or less fixed in space with time. A detailed discussion of these observations is given in Bessler (1984).

In support of our characterization of the wake in figure 7 is a photograph by Calderbank (1967) of a circularly capped CO_2 bubble rising in water at high Re. The lower right-hand photograph in his figure 15A shows a free shear layer originating at the bubble's rim and terminating in a shed vortex. The vortex shed just before the one forming is also shown. It is clearly larger in size than the one forming, indicating (as we show in figure 7) growth of the shed vortex. A free shear layer is also visible in his figure 15B for a CO_2 bubble rising in a 1% aqueous solution of carboxymethylcellulose.

Our use of a Walters & Davidson (1962) plunger-type injector prevents bubble rocking and produces the cusp-shaped primary wake that we observe. The dump cup

injector used by Crabtree & Bridgwater (1967) and the cup injector used by Lindt (1972) impart rocking to the bubble, producing an open helical vortex street wake. The rubber flap injector used by Collins (1965*a*, *b*) generated a bubble that did not rock.

Although the injector has considerable effect on the shape of the primary wake, the growth of the shed vortices and their formation in the free shear layer seem common to all high *Re* bubbles.

4. Structure of the wake

The assumption of irrotational flow over a sphere with a constant pressure along the bubble cap was successful in predicting the rise velocity of a spherical-cap bubble when the radius of the sphere matched the curvature of the bubble cap (Davies & Taylor 1950). Lazarek & Littman (1974) found that the pressure field in front of the circularly capped bubble and on the bubble cap was well approximated by irrotational flow around an oval body. They found relatively poor agreement of the experimental pressure field with the irrotational-flow prediction when the wake boundary was a cylinder or had an extremely long axial length. This is not surprising since the experimentally observed primary wake shape, shown in figure 6, more closely resembles an airfoil than an oval body. The airfoil shape agrees with the arguments of Batchelor (1956*a*, *b*) who stated that the primary wake should theoretically have a cusped tail in order to permit a uniform velocity just outside of the downstream end of the primary-wake bounding streamline. Batchelor further argued that the primary wake should be closed in order to satisfy the boundary condition of uniform velocity far downstream from the bubble.

The fluid inside the closed primary wake is driven by the action of viscous stresses at the vortex sheet which are generated by the upward motion of the bubble. In response to these driving forces, Batchelor reasoned that two standing eddies should exist within the primary wake, having uniform vorticity and opposite sense of rotation. This is supported by the work of Collins (1966).

5. Shape of the bubble and primary wake

The airfoil shape suggests the use of the Joukowski transformation as a means of generating the primary-wake boundary and figure 8(*a*) shows the mapping

$$z = \zeta + \left(\frac{\lambda^2}{\zeta}\right), \tag{4.1}$$

where

$$\zeta = c - \lambda + c\,\mathrm{e}^{i\theta}, \tag{4.2}$$

on the circle of radius c. Points on this circle in the ζ-plane are mapped to the primary-wake boundary in the z-plane using the auxiliary equations

$$z = \xi\left[1 + \frac{\lambda^2}{|\zeta^2|}\right], \tag{4.3}$$

$$y = \eta\left[1 - \frac{\lambda^2}{|\zeta^2|}\right] \tag{4.4}$$

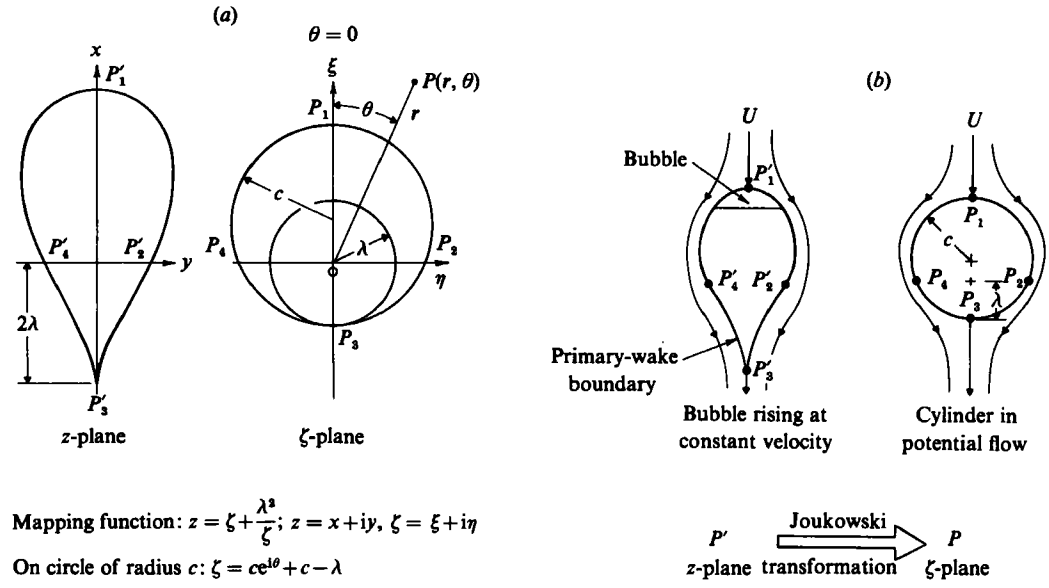

FIGURE 8. (*a*) The Joukowski transformation for mapping a circle into an airfoil. (*b*) Conformal mapping of the bubble cap and primary-wake boundary by the Joukowski transformation.

	Axial location, x/a			
	0	−1.0	−2.0	−3.0
$y/a = 0$				
Experimental	0.97	0.56	0.30	0.17
Predicted	1.0	0.60	0.33	0.15
$y/a = 0.43$				
Experimental	0.65	0.48	0.26	0.16
Predicted	0.70	0.53	0.29	0.14
$y/a = 0.87$				
Experimental	0.35	0.39	0.25	0.15
Predicted	0.32	0.42	0.28	0.13
$y/a = 1.74$				
Experimental	−0.16	0.11	0.12	0.10
Predicted	−0.18	0.15	0.13	0.10

TABLE 4. Comparison between experimental and predicted frontal pressure coefficients

obtained by equating the real and imaginary parts of (4.1). Offset of the circle in the ζ-plane is chosen by requiring the circle of radius c to be tangent to the circle of radius λ at P_3 in figure 8(*a*). This results in a cusped tail for the Joukowski profile. The value of c is essentially a size scaling factor when the aforementioned method of determining the offset is used. Therefore, c was chosen to be unity and λ varied to find the shape of the bubble cap that produced agreement between the experimental and potential-flow pressures along the cap. A value of $\lambda = 0.6$ gave excellent results for circularly capped bubbles.

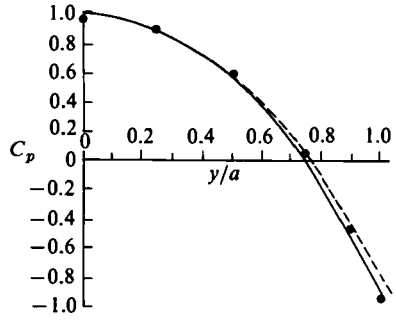

• Measured experimental cap pressure
— Predicted pressure from conformal mapping of irrotational flow around a cylinder
--- The Davies & Taylor constant-pressure boundary condition

FIGURE 9. Comparison of the experimental and predicted pressures along the bubble cap for a bubble rising in water.

The use of the Joukowski mapping with $\lambda = 0.6$ to define the bubble and the primary-wake boundary also was found to yield good agreement with the flow visualization photographs in terms of wake length and shape. This shape was, therefore, used to model the bubble and its closed primary wake rising up through the fluid in the column. Matching of the experimental and potential-flow pressures along the bubble cap was done as follows.

The complex potential w in the ζ-plane for flow around a cylinder of radius c with a far field velocity $-U$ as pictured in figure 8(*b*), is given by

$$w = -U\left(\zeta + \frac{c^2}{\zeta}\right); \quad \zeta = \xi + \mathrm{i}\eta. \tag{4.5}$$

In order to obtain the pressure coefficient from its definition, (3.1), the pressure field was calculated from the steady form of Bernoulli's equation referred to axes moving with the bubble, giving

$$C_p = 1 - \left[\sin^2\theta\left(1+\frac{c^2}{r^2}\right)^2 + \cos^2\theta\left(1-\frac{c^2}{r^2}\right)^2\right]\left|\frac{\zeta^2}{\zeta-\lambda^2}\right|^2, \tag{4.6}$$

where the terms in the equation are defined in figure 8*a*.

The experimental pressure-coefficient data in the field above the bubble show excellent agreement with the predictions of (4.6) as seen in table 4, verifying the work of Lazarek & Littman (1974) that this portion of the flow field is irrotational.

The theoretical expression for the pressure coefficient along the bubble cap was derived by the method of Davies & Taylor (1950) as

$$C_p = 1 - \frac{2gx}{U^2}, \tag{4.7}$$

where x is the vertical distance beneath the stagnation point of the bubble. Figure 9 shows the excellent agreement between (4.6), (4.7) and the experimental data for a bubble rising in pure water. Further details of this comparison are given in Bessler (1984).

REFERENCES

BATCHELOR, G. K. 1956*a* On steady laminar flow with closed streamlines at high Reynolds number. *J. Fluid Mech.* **1**, 177.

BATCHELOR, G. K. 1956*b* A proposal concerning laminar wakes behind bluff bodies at large Reynolds number. *J. Fluid Mech.* **1**, 388.

BATCHELOR, G. K. 1967 *An Introduction to Fluid Dynamics.* Cambridge University Press.

BESSLER, W. F. 1984 Analytical and experimental studies of wakes behind circularly capped bubbles. Ph.D. thesis, Rensselaer Polytechnic Institute, Troy, NY.

CALDERBANK, P. H. 1967 Gas absorption from bubbles. *The Chemical Engineer* No. 212, CE 209.

CLIFT, R., GRACE, J. R. & WEBER, M. E. 1978 *Bubbles, Drops and Particles.* Academic.

COLLINS, R. 1965*a* Structure and behaviour of wakes behind two dimensional air bubbles in water. *Chem. Engng Sci.* **20**, 851.

COLLINS, R. 1965*b* A simple model of a plane gas bubble in a liquid. *J. Fluid Mech.* **22**, 763.

COLLINS, R. 1966 A second approximation for the velocity of a large gas bubble rising in an infinite liquid. *J. Fluid Mech.* **25**, 469.

COLLINS, R. 1974 Models of spherical-cap bubbles. In *Proc. Int. Coll. on Bubbles and Drops. Cal. Inst. Tech. and Jet Prop. Lab., 28–30 Aug. 1974,* Vol. II, pp. 414.

COPPUS, J. H. C., RIETEMA, K. & OTTENGRAF, S. P. P. 1977 Wake phenomena behind spherical-cap bubbles and solid spherical cap bodies. *Trans. Instn Chem. Engrs* **55**, 122.

CRABTREE, J. R. & BRIDGWATER, J. 1967 The wakes behind two dimensional air bubbles. *Chem. Engng Sci.* **22**, 1517.

DAVIES, R. M. & TAYLOR, G. I. 1950 The mechanics of large bubbles rising through extended liquids and through liquids in tubes. *Proc. R. Soc. Lond.* **A200**, 375.

HABERMAN, W. L. & MORTON, R. K. 1953 An experimental investigation of the drag and shape of air bubbles rising in various liquids. *David Taylor Model Basin Rep.* 802, NS715–102.

HARPER, J. F. 1972 The motion of bubbles and drops through liquids. *Adv. Appl. Mech.* **12**, 59.

HILLS, J. 1975 The two-dimensional elliptical cap bubble. *J. Fluid Mech.* **68**, 503.

LAZAREK, G. M. 1972 Pressure fields due to large circularly capped air bubbles rising in water. Ph.D. thesis, Rensselaer Polytechnic Institute, Troy, NY.

LAZAREK, G. M. & LITTMAN, H. 1974 The pressure field due to a large circular-capped air bubble rising in water. *J. Fluid Mech.* **66**, 673.

LINDT, J. T. 1972 On the periodic nature of the drag on a rising bubble. *Chem. Engng Sci.* **27**, 1775.

MANIERI, C. C. & MENDELSON, H. D. 1968 The rise velocity of bubbles in tubes and rectangular channels. *AIChE J.* **14**, 295.

MAXWORTHY, T. 1967 A note on the existence of wakes behind large rising bubbles. *J. Fluid Mech.* **27**, 368.

MOORE, D. W. 1959 The rise of a gas bubble in a viscous liquid. *J. Fluid Mech.* **6**, 113.

RIPPIN, D. W. & DAVIDSON, J. F. 1967 Free streamline theory for a large gas bubble in a liquid. *Chem. Engng Sci.* **22**, 217.

RYSKIN, G. & LEAL, L. G. 1984 Numerical solution of free-boundary problems in fluid mechanics. Part 2. Buoyancy-driven motion of a gas bubble through a quiescent liquid. *J. Fluid Mech.* **148**, 19.

SAFFMAN, P. G. & TANVEER, S. 1984 Prandlt–Batchelor flow past a flat plate with a forward-facing flap. *J. Fluid Mech.* **143**, 351.

SLAUGHTER, I. & WRAITH, A. E. 1968 The wake of a large gas bubble. *Chem. Engng Sci.* **23**, 932.

WALTERS, J. K. & DAVIDSON, J. F. 1962 The initial motion of a gas bubble formed in an inviscid liquid. Part 1. The two-dimensional bubble. *J. Fluid Mech.* **12**, 408.

WEGENER, P. P. & PARLANGE, J. Y. 1973 Spherical-cap bubbles. *Ann. Rev. Fluid Mech.* **4**, 79.

WEGENER, P. P., SUNDELL, R. E. & PARLANGE, J. Y. 1971 Spherical cap bubbles rising in liquids. *Z. Flugwiss.* **19**, 247.